Journal of Materials Chemistry A

RSC Publishing

PAPER

View Article Online
View Journal | View Issue

UV irradiation synthesis of an Au–graphene nanocomposite with enhanced electrochemical sensing properties†

Cite this: *J. Mater. Chem. A*, 2013, **1**, 9189

Ping Wang,‡[ab] Zhong-Gang Liu,‡[ab] Xing Chen,[b] Fan-Li Meng,[b] Jin-Huai Liu[b] and Xing-Jiu Huang*[ab]

Received 23rd March 2013
Accepted 23rd May 2013

DOI: 10.1039/c3ta11155e

www.rsc.org/MaterialsA

A facile and environmentally friendly strategy using UV irradiation has been successfully developed for the preparation of an Au–reduced graphene oxide (Au–RGO) nanocomposite. The as-prepared nanocomposite was analysed and characterized by scanning electron microscopy (SEM), transmission electron microscopy (TEM), Raman spectroscopy, UV-Vis absorption spectroscopy and X-ray photoelectron spectroscopy (XPS). The results demonstrated that the simultaneous reduction of graphene oxide and formation of Au nanoparticles were achieved. The obtained Au nanoparticles with an average diameter of 25.7 nm were uniformly dispersed on graphene sheets. The introduction of Au nanoparticles has efficiently maximized the electroactive surface area of catalysts and the conductivity of the Au–RGO nanocomposite. The graphene sheets not only provided the nucleation sites but also prevented the Au nanoparticles from agglomerating. Moreover, in order to illuminate the advantages of the Au–RGO nanocomposite, its electrochemical sensing performance toward TNT as an example has been further investigated by cyclic voltammetry (CV) and linear scan voltammetry (LSV). The results confirmed that the Au–RGO nanocomposite exhibited much better electrocatalytic activity toward TNT than RGO and holds great promise for developing as an electrochemical sensor.

Introduction

Graphene, as a "rising star" material, has received considerable attention due to its large specific surface area, as well as intriguing physical properties (electronic, mechanical and thermal).[1–5] Most of the graphene used was produced from the reduction of graphene oxide and usually had functional groups such as hydroxyl and carboxyl. The reduction of water-dispersed graphene oxide (GO) resulted in a significant decrease in their hydrophilic character and consequently led to their irreversible agglomeration and precipitation because of the van der Waals and π–π stacking interactions between individual graphene sheets.[6,7] This was recognized to significantly affect the practical applications of graphene.

The clever introduction of metal nanoparticles onto graphene can effectively separate the graphene sheets and prevent the aggregating inclination of metal nanoparticles.[8] Enlightened by these advantages, much more attention has been paid to exploring metal–graphene nanocomposites. In particular, Au nanoparticles,[9–17] as typical noble metal nanoparticles, have been introduced due to their extraordinary conductivity and excellent catalysis. So far, many approaches have been attempted for the preparation of Au–graphene nanocomposites, which include chemical reduction processes,[10–13] hydrothermal techniques,[15] physical vapor deposition[16] and *ex situ* approaches based on covalent interaction[17] and electrostatic interaction.[18] Although, in these methods, Au nanoparticles can be dispersed on graphene sheets with relatively high density, these obviously involved highly toxic chemicals or high temperature, and complicated manipulations were required. Some of them may cause the possible contamination of the nanocomposites, thereby reducing the electron transfer capacity and catalytic activity. Therefore, it is of much interest and significance to develop a facile and environment-friendly strategy for the synthesis of Au–graphene nanocomposites with improved catalytic activity. Photochemical reduction, as one "green" and reductant-free technique, can be appropriate for this objective. Very recently, a series of excellent results with photochemical reduction techniques on the reduction of graphene oxide and Au nanoparticles have been obtained.[19–25] In particular, Huang *et al.* reported the controlled synthesis of anisotropic Au nanostructure through TiO_2-assisted photochemical reduction.[20]

[a]*Department of Chemistry, University of Science and Technology of China, Hefei 230026, PR China. E-mail: xingjiuhuang@iim.ac.cn; Fax: +86 551 65592420; Tel: +86 551 65591167*

[b]*Laboratory of Nanomaterials and Environmental Detection, Hefei Institute of Physical Sciences, Chinese Academy of Sciences, Hefei 230031, PR China*

† Electronic supplementary information (ESI) available: The typical AFM image of GO, SEM of GO and Au-RGO, measurements stability of Au-RGO modified GCE in 0.5 M H_2SO_4. See DOI: 10.1039/c3ta11155e

‡ These authors contributed equally to this work.

Kim *et al.* found that reversible formation and dissolution of gold nanoparticles were achieved by UV irradiation.[22] Eustis *et al.* obtained Au nanoparticles from the photochemical reduction of Au^{3+} in the presence of poly(vinyl-pyrrolidone) (PVP) and ethylene glycol (EG).[23] And also, the approach has been employed to synthesize the reduced graphene oxide sheet by Ding and Matsumoto *et al.*[24,25] Even though preliminary studies on the synthesis of Au–graphene nanocomposite have been carried out, the nanocomposite was prepared in organic solvent by using phosphotungstate as a photocatalyst,[26] where it was difficult to separate the photocatalyst from the graphene sheets due to the interaction between them. Moreover, the electrocatalytic performance of the nanocomposite prepared by this method has not been evaluated.[27,28]

In this work, we present UV irradiation as a facile approach to prepare an Au–reduced graphene oxide (Au–RGO) nanocomposite under mild conditions. The simultaneous reduction of graphene oxide and formation of Au nanoparticles were realized. The obtained Au nanoparticles were uniformly dispersed on graphene sheets without agglomeration. The conductivity of the nanocomposite was highly improved. The as-prepared nanocomposite was expected to have good electrochemical activity. Herein, by employing the detection of 2,4,6-trinitrotoluene (TNT) as an example, the electrocatalytic properties of Au–RGO were further evaluated. The results strongly indicated that the as-prepared nanocomposite showed good electrochemical sensing performance.

Experimental section

Chemical reagents

All reagents were purchased from Sinopharm Chemical Reagent Co., Ltd. (China) and were of analytical grade. 0.5 M phosphate buffer solution (PBS) was used as a supporting electrolyte. Ultrapure fresh water was obtained from a Millipore water purification system (MilliQ, specific resistivity >18 MΩ cm, S.A., Molsheim, France) and used in all runs.

Preparation of graphene oxide sheets

The aqueous graphene oxide (GO) dispersion was prepared by oxidizing graphite according to a modified Hummer's method.[29] Briefly, 1 g of graphite powder, 1 g of $NaNO_3$ and 46 mL of concentrated H_2SO_4 were mixed and stirred for 30 min in an ice bath, followed by the slow addition of 6 g of $KMnO_4$. After another 30 min, the flask was transferred to an oil bath and stirred at 35 °C for 2 h. 92 mL of deionized water was further added to the flask and allowed to react at 90 °C for 30 min. Then 200 mL of deionized water and 6 mL of H_2O_2 were added. The colour of the solution changed from brown to light yellow. The warm solution was filtered and purified with 5% HCl and water multiple times.

Preparation of the Au–reduced graphene oxide nanocomposite

The Au–reduced graphene oxide (Au–RGO) nanocomposite was synthesized by UV light irradiation. The procedures employed for preparing the nanocomposite were as follows. The synthesized graphite oxide dispersion was firstly exfoliated for 1 h to form single- or few-layered graphene oxide (0.15 mg mL^{-1}) by ultrasonication (100 W). Subsequently, *N*-hexadecyltrimethylammonium chloride (CTAC) was added into 20 mL of GO homogenous solution and stirred for 0.5 h to completely dissolve CTAC. The final concentration of CTAC was 0.02 M. 0.8 mL $HAuCl_4$ (1.0 wt% in water) was dripped into the mixture. The solution was then irradiated (mercury lamp, 300 W) for 5 h under continuous stirring. The formed Au–RGO nanocomposite suspensions were repeatedly centrifuged at 10 000 rpm to remove CTAC and free Au nanoparticles. Reduced graphene oxide (RGO) was also synthesized using the same process without using $HAuCl_4$.

Characterization

Scanning electron microscopy (SEM) images were obtained with a FEI Quanta 200 FEG field emission scanning electron microscope. Transmission electron microscopy (TEM) and high-resolution TEM (HRTEM) analyses were performed using a JEM-2010 microscopy operated at an accelerating voltage of 200 kV. X-ray photoelectron spectroscopy (XPS) analysis was conducted on a ESCAlab MKII spectrometer using Al Kα as the irradiation source. UV-Vis spectra were measured with a UV 2550 spectrophotometer (Shimadzu, Japan). Atomic force microscopy (AFM) images were taken by a Nanoscope V Multimode scanning probe microscopy. Raman spectra were collected from a Lab-RAM HR 800 confocal microscope Raman system using laser 532 nm.

The electrochemical experiments were recorded using a CHI 660D computer-controlled potentiostat (ChenHua Instruments Co., Shanghai, China) with a standard three-electrode system. A conventional three-electrode system consisted of a glassy carbon working electrode (GCE, 3 mm diameter), Ag/AgCl as the reference electrode and a platinum wire as the counter electrode.

Electrochemical measurements

Before each modification, the bare glassy carbon electrode was sequentially polished with 0.3 μm and 0.05 μm alumina power slurries to a mirror-shiny surface and then sonicated with HNO_3 solution (v/v, 1 : 1), absolute ethanol and deionized water, respectively. Then, 4.0 μL of Au–RGO ethanol solution (3 mg mL^{-1}) was dripped onto the surface of a freshly polished glassy carbon electrode and allowed to dry at room temperature. The GO, RGO modified GCE were prepared using the same process for comparison.

Cyclic voltammetry (CV) and linear scan voltammetry (LSV) were used for the electrochemical detection of 2,4,6-trinitrotoluene (TNT) in 0.5 M PBS under optimized conditions. TNT was preconcentrated from the stirred solution and placed on the surface of the GCE for 120 s. Reductive stripping responses were recorded between 0.4 and −0.8 V with a scan rate of 100 mV s^{-1}. High-purity nitrogen gas was bubbled into the electrolyte before the electrochemical experiment to thoroughly remove dissolved oxygen.

Results and discussion

Fig. 1 shows the TEM images of the as-prepared Au–RGO nanocomposite. It can be clearly seen that high-density Au nanoparticles were uniformly dispersed on the reduced graphene oxide (RGO) sheets with negligible aggregation. No free nanoparticles were observed outside the graphene sheets even after intensive sonication during the preparation of the sample for characterization. This demonstrated the strong interaction between the graphene sheets and the Au nanoparticles. The transparent and thin RGO sheets can be distinguished from the backgrounds with indistinct corrugation nature. No obvious partial overlap and coalescence of the RGO sheets occurred. A HRTEM image of the Au nanoparticles is presented in the right-top inset of Fig. 1b. The lattice fringes with a lattice spacing of about 0.235 nm were corresponding to the (111) plane of face center cubic (fcc) structure of Au nanoparticles. Furthermore, the interface between the RGO sheets and the Au nanoparticles can be clearly observed, indicating that Au nanoparticles were well anchored on the surfaces of the sheets. The size distribution (right-bottom inset of Fig. 1b) shows that Au nanoparticles were relatively uniform with diameters around 25.7 nm.

Raman spectroscopy gives useful information related to the electronic and structural properties of graphene. Fig. 2 shows Raman spectra of graphite, GO, and the Au–RGO nanocomposite. The D band (~1330 cm^{-1}) is related to the defect induced breathing mode of A_{1g} symmetry and the G band (~1580 cm^{-1}) is of E_{2g} symmetry, representing the relative degree of graphitization. In comparison to the Raman spectrum of graphite, the G bands of GO and Au–RGO were broadened because of the enhanced isolated double bonds and the D bands became outstanding due to the enhanced disorder with GO and Au–RGO. The G band of the Au–RGO nanocomposite (1601 cm^{-1}) was obviously upshifted by 11 cm^{-1} with respect to GO (1590 cm^{-1}), which is consistent with previous research that Au introduced would cause upshift of the G band due to the electron–phonon coupling.[30] The intensity ratio of the D to G bands (I_D/I_G) is often used as a measure of defect levels in graphitic systems. With the oxidization of graphite, the ratio of I_D/I_G actually increased to 1.09, demonstrating the formation of large sp^3 domain.[31] Integrating the AFM results (Fig. S1†), it was believed that GO sheets were efficiently oxidized and exploited, and single or few layers with the average thickness of about 1.0 nm were formed. In addition, the dimension of GO sheets was several micrometres, which could provide a satisfactory scaffold for loading metal particles. When GO was reduced to RGO, the ratio of I_D/I_G actually increased from 1.09 to 1.22 following UV treatment, indicating that the size of the sp^2 domain decreased as the graphene sheet was broken into fragments during the UV treatment. The 2D band is well-known as a key parameter to distinguish the thickness of the graphene sheets. For reduction by UV irradiation, a broad 2D band at 2632 cm^{-1} for Au-RGO nanocomposite was observed, confirming the presence of few layers graphene sheets in the as-prepared nanocomposite.

Fig. 3a presents the XPS survey spectra of graphene oxide and Au–reduced graphene oxide nanocomposite, which exhibited

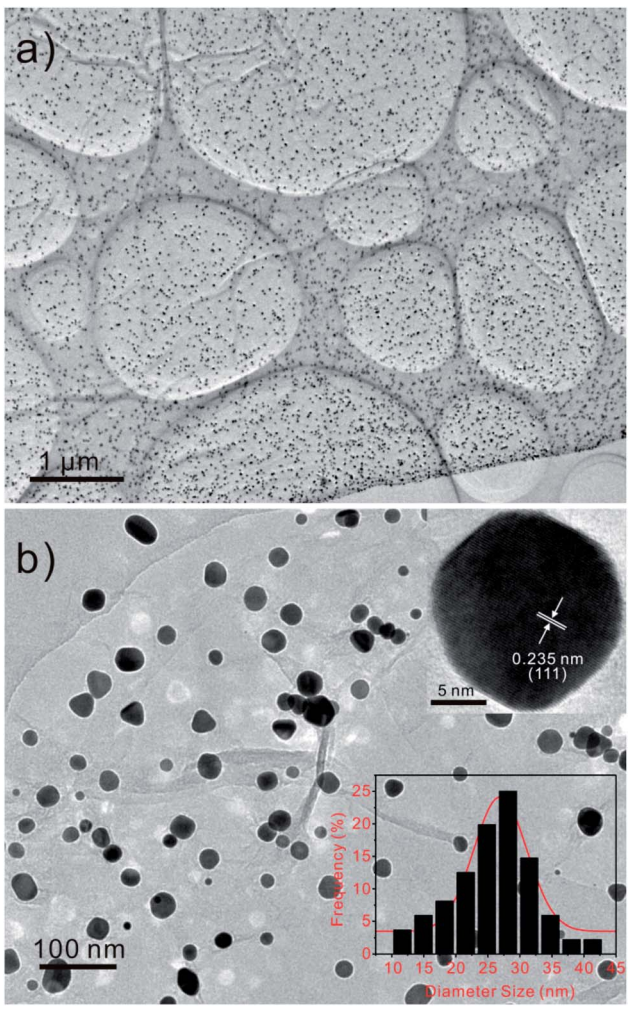

Fig. 1 (a and b) TEM images of Au-reduced graphene oxide nanocomposite. The right-top inset shown in (b) presents a HRTEM image of an Au nanoparticle and the right-bottom is the statistical distribution of diameter size for Au nanoparticles anchored on the reduced graphene sheets.

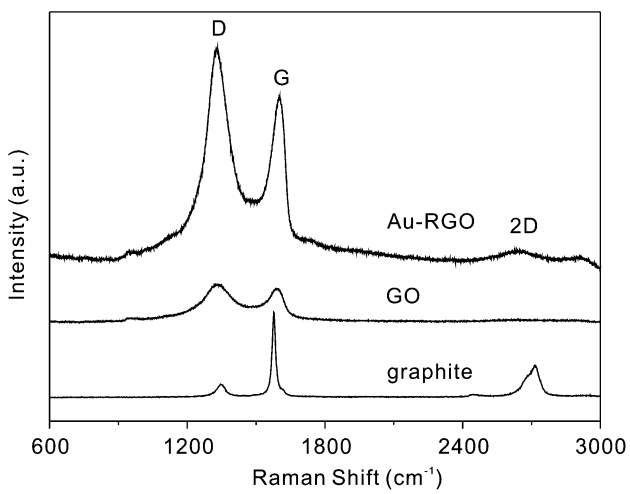

Fig. 2 Raman spectra of graphite, graphene oxide (GO) and Au-reduced graphene oxide (Au–RGO) nanocomposite.

peaks associated with C 1s, O 1s. Compared with the XPS spectra of graphene oxide, the peak associated with C 1s became predominant, while the peak related to O 1s was greatly weakened, indicating that graphene oxide was deoxygenated and reduced to form the Au–RGO nanocomposite. The peak of Au evidently emerged for RGO sheets decorated with Au nanoparticles after UV irradiation. The change in morphology was also characterized by SEM (Fig. S2†). A large amount of Au nanoparticles were observed on the surface of the clean graphene sheets. In addition, there were no peaks of other elements except C, O and Au in the X-ray photoelectron spectrum of Au–RGO, indicating the high purity of the as-prepared nanocomposite. In the high-resolution XPS spectrum presented in Fig. 3b, the Au $4f_{7/2}$ and Au $4f_{5/2}$ peaks were centered at 83.7 eV and 87.0 eV, respectively, which were in agreement with the widely reported XPS spectra of metallic Au^0 at 84.0 eV and 87.7 eV.[32] Clearly it can be further concluded that Au^{3+} ions have been effectively reduced on the surface of graphene oxide sheets. A blue shift of Au 4f resulted from the electron transfer from graphene to Au NPs.[15] It is known that graphene sheets obtained by UV reduction of GO contain numerous carbon vacancies and defects, which can lead to a strong chemical interaction between Au NPs and graphene sheets.[33] We found a blue shift of O 1s in the high-resolution XPS spectra (Fig. S3†). Combined with the blue shift of Au 4f, it can be demonstrated the Au–RGO was a covalent hybrid and a strong chemical interaction between Au NPs and graphene sheets.[34] High resolution spectra in the region of the C1s characteristic peak for GO and Au–RGO nanocomposite are shown in Fig. 3c and d, which involved contributions from various carbon–oxygen binding arrangements. After UV treatment, the peak corresponding to the sp^2 carbon at 284.5 eV was the major feature of the C 1s region. While the intensity of the sp^3 carbon peak at 285.6 eV was considerably reduced. This indicated the significant restoration of the graphitic lattice. The prominent peak at higher binding energies in the GO C 1s region is due to the spectral contributions from oxygen functionalities. The intensities of epoxy groups (286.7 eV), carboxyl (287.1 eV) and carbonyl groups (288.6 eV) compared to the sp^2 carbon peak (284.5 eV) were remarkably reduced after UV treatment. It was further confirmed that UV treatment significantly affected the functional groups of carbon and the majority of the conjugated graphene networks was restored.

In order to understand the formation mechanism of the Au–reduced graphene oxide nanocomposite, time-dependent reactions have been examined. Fig. 4 shows the typical UV-Vis absorption spectra of the Au–RGO nanocomposite as a function of time. The absorption spectroscopy was applied to monitor the morphology, diameter and polydiversity of Au nanoparticle from the position and width of surface plasmon resonance (SPR).[35] It was observed that a peak for Au nanoparticles at 546 nm (ref. 36) appeared after 1 h of UV irradiation, and its intensity increased with irradiation time. The strong and symmetric band can be attributed to the characteristic peaks of the Au nanoparticles.[37] In addition, a slight red colour of the suspension was observed. Therefore, monodispersed Au nanoparticles anchored on graphene sheets have formed from free Au^{3+} ions. The formation process can be explained as follows. During the UV irradiation process, graphene oxide can accept photo-excited electrons, which have a strong reducing ability. These electrons in graphene oxide caused the reduction of Au^{3+} to Au^0, following by nucleation of Au^0 on the surface of graphene.[26] Moreover, the cationic CTAC can efficiently prevent agglomeration and precipitation of Au^{3+} ions and form monodispersed Au nanoparticles onto the graphene oxide sheets during photochemical process.[36] At the same time, the UV irradiation caused the detachment of oxygen-containing functional groups, leading to the reduction of graphene oxide. This has been verified with XPS analysis. Note that when the irradiation time was beyond 5 h, Au nanoparticles with irregular morphology were observed and tended to agglomerate. Thus, an irradiation time of 5 h was employed for the preparation of the nanocomposite.

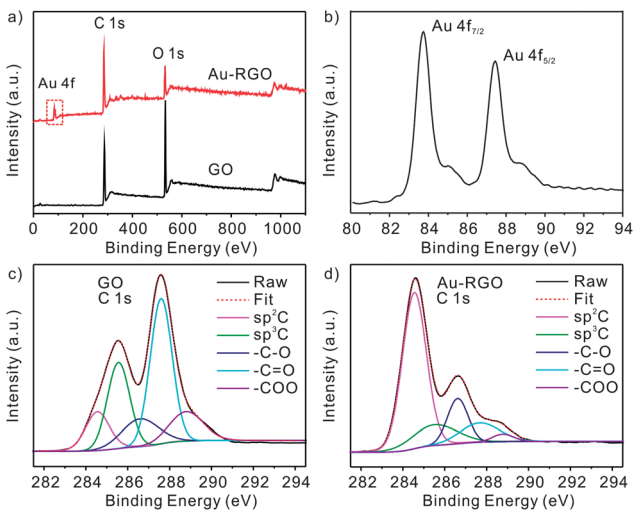

Fig. 3 (a) XPS spectra of graphene oxide (GO) and the Au–reduced graphene oxide (Au–RGO) nanocomposite. (b) High-resolution XPS spectrum of Au 4f pattern for Au–reduced graphene oxide nanocomposite. High-resolution spectra of C 1s of (c) GO and (d) Au–RGO nanocomposite.

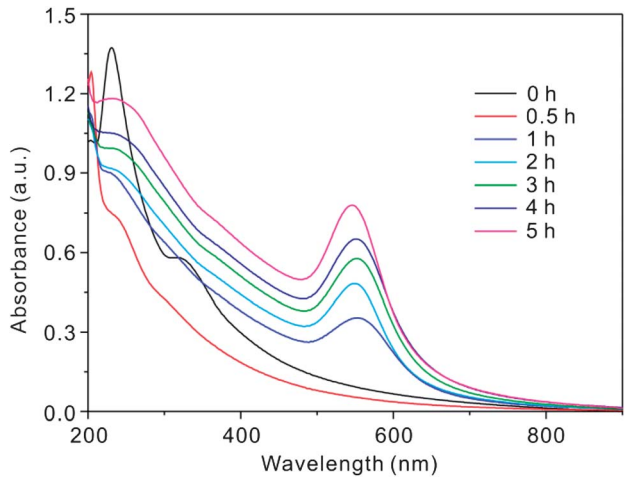

Fig. 4 UV-Vis absorption spectra of Au–reduced graphene oxide nanocomposite during UV irradiation recorded as a function of irradiation time.

It is well-known that the reduction of graphene oxide sheets tends to form irreversible agglomerates and even restack to form graphite, which is due to the van der Waals and π–π stacking interactions between individual graphene sheets.[6,7] However, in the present work, the uniform Au nanoparticles embedded between the exfoliated graphene sheets can serve as stabilizers and RGO sheets well dispersed in ethanol solution can also be obtained. In turn, graphene sheets can not only provide the nucleation sites but also prevent the Au nanoparticles from agglomerating. It is worth pointing out that UV irradiation was clearly demonstrated to be an efficient reductant to synthesize Au–RGO nanocomposite.[26]

The fabricated Au–RGO nanocomposite modified GCE was firstly electrochemically characterized using cyclic voltammetry. Fig. 5 presents the comparison of cyclic voltammetric responses of the bare, and graphene oxide (GO), reduced graphene oxide (RGO) and Au–RGO nanocomposite modified electrodes. Compared with the bare electrode, the anodic and cathodic peaks almost disappeared on graphene oxide modified electrode. This was attributed to there being plenty of functional groups, including hydroxyl and carboxyl groups, in GO, which blocked the diffusion of $Fe(CN)_6^{3-/4-}$ to the electrode surface and hindered the electron and mass transfer. In contrast, the response of the RGO modified electrode was increased compared to that of GO, suggesting that the electrochemical activity of the graphene sheets was remarkably improved after UV irradiation reduction. However, the RGO modified electrode showed weaker current peaks than bare GCE, indicating that the oxygen-related defects remained in the RGO sheets.[38] After modifying with the Au–RGO nanocomposite, the electrode showed the best electrochemical performance. This revealed that the highly conducting Au nanoparticles can provide the necessary conduction pathways on the electrode surface and a better electrochemical catalytic behavior, resulting in the promotion of electron transfer process at the modified electrode surface.[38,39] Moreover, the Au–RGO nanocomposite modified electrode was also evaluated in 0.5 M H_2SO_4 (inset in Fig. S4†) and displayed a characteristic reduction peak for Au nanoparticles at ~0.92 V,[40] indicating that Au nanoparticles were formed on the graphene sheets by the UV treatment. Meanwhile, we further evaluated the measurement stability of Au-reduced graphene oxide nanocomposite modified GCE (Fig. S4†). No obvious change of the characteristic reduction peak for Au nanoparticles was observed with the relative standard deviation (RSD) 7.63%, indicating the robust durability of the modified electrode and the stable composition of Au–RGO nanocomposite.

In order to evaluate the electrochemical sensing properties of as-prepared Au–RGO modified electrode, here the detection of 2,4,6-trinitrotoluene (TNT) was performed as an example. Fig. 6 presents the CV analytical characteristics for 700 μg L^{-1} of TNT on bare, RGO, and Au–RGO modified electrode in 0.5 M PBS (pH 7.0). As expected, no reduction response of TNT was showed on bare GCE. However, three relative weaker peaks at −0.37, −0.51 and −0.62 V of TNT on RGO modified electrode can be observed, which was due to the interaction between RGO and aromatic molecules *via* strong π–π covalent stacking.[41,42] Note that the three peaks can be assigned to sequential reduction of the three nitro groups into amine groups by the conversion of hydroxylamine through the $6e^-$ transfer process.[43] In comparison, it was found that three well-defined peaks were represented on the Au–RGO modified electrode with the positive shift of peak potential (−0.35, −0.49, −0.59 V). The much better electrochemical performance of the Au–RGO modified electrode toward TNT revealed the fact that the combination of Au nanoparticles and RGO sheets can not only improve the conductivity but also provide the excellent catalytic activity.

The electrochemical measurements toward TNT on Au-RGO and RGO modified electrode were performed using linear scan voltammetry (LSV) under the same experimental conditions. It can be observed in Fig. 7 that the peak currents of TNT on Au–RGO modified electrode increased in a linear manner against its

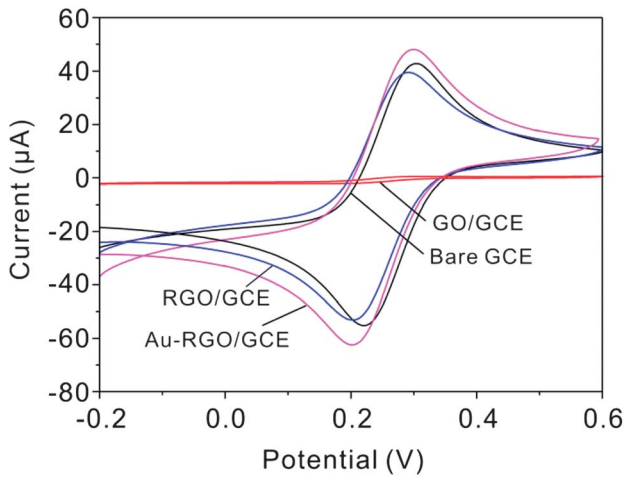

Fig. 5 Cyclic voltammograms of the bare electrode, and graphene oxide, reduced graphene oxide and Au–reduced graphene oxide nanocomposite modified electrodes in 5.0 mM $Fe(CN)_6^{3-/4-}$ solution containing 0.1 M KCl. Scan rate is 100 mV s^{-1}.

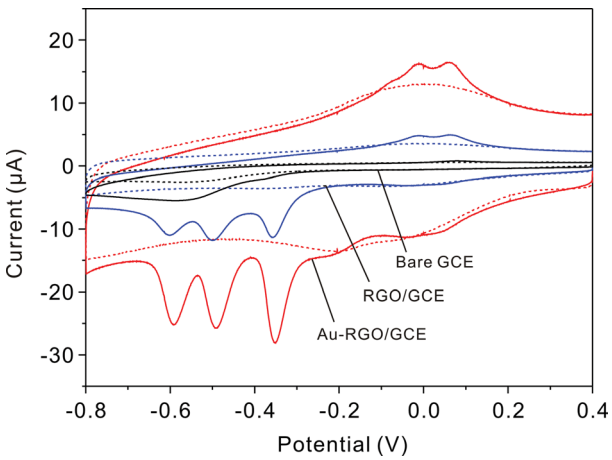

Fig. 6 Cyclic voltammetric responses for TNT (700 μg L^{-1}) on bare GCE, and RGO and Au–RGO modified electrode in 0.5 M PBS (pH 7.0). The dotted lines refer to the corresponding baselines.

concentrations. The linearization equation was $i/\mu A = 0.12 + 0.023c/\mu g\ L^{-1}$ (Fig. 7), with a limit of detection (LOD) of 5.9 $\mu g\ L^{-1}$ (3σ method), where the peak currents were recorded with reduction peak at −0.35 V. The stripping voltammograms for TNT at concentrations of 20–700 ppb are given in Fig. 7 (right-top inset). Meanwhile, The LSV responses for TNT at concentrations of 70–700 ppb are also shown in Fig. 7 (right-bottom inset). The linearization equation was $i/\mu A = 0.98 + 0.0075c/\mu g\ L^{-1}$ with a detection limit of 11.5 $\mu g\ L^{-1}$ (3σ method). The results demonstrated that the good sensitivity and detection limit obtained on Au–RGO modified electrode were found to be superior to that of RGO. As discussed above, it was recognized that the synergistic contribution of the efficient conductivity of RGO and high loading of Au nanoparticles on RGO sheets should be responsible for the enhanced electrochemical activity. Graphene sheets with high adsorption capacity toward TNT *via* π–π stacking interaction were favourable for accumulation of TNT in the preconcentration process. The improved conductivity of the RGO after UV treatment and high electrocatalytic activity of Au nanoparticles facilitated the redox reaction TNT molecules. It is thus expected that the Au–RGO nanocomposite can be favourable for enhanced electrochemical platform for TNT detection.

The selectivity of the Au–RGO modified electrode was developed by detecting several aromatic compounds and the results are summarized in Table 1. No electrochemical response to nitro-free compounds on the Au–RGO modified electrode can be found, even with higher concentration (2000 $\mu g\ L^{-1}$). However, the Au–RGO modified electrode showed obvious responses to nitro-aromatic compounds. For 2,4-dinitrotoluene (2,4-DNT), there were two reduction responses at −0.53 V and −0.67 V. While for 4-nitrotoluene (4-NT) and 4-nitrophenol (4-NP), a single reduction response can be observed at −0.67 V and −0.73 V, respectively. Moreover, three stronger reduction responses of TNT on Au–RGO modified electrode can be clearly seen even at lower concentrations. We suggest that the difference may be attributed to nitro groups and electron properties. It has to recognized that the actual and reasonable reason for this is unclear at the present stage and further research is needed to elucidate it. Briefly, the results demonstrated that the Au–RGO modified electrode can show favourable selectivity for TNT.

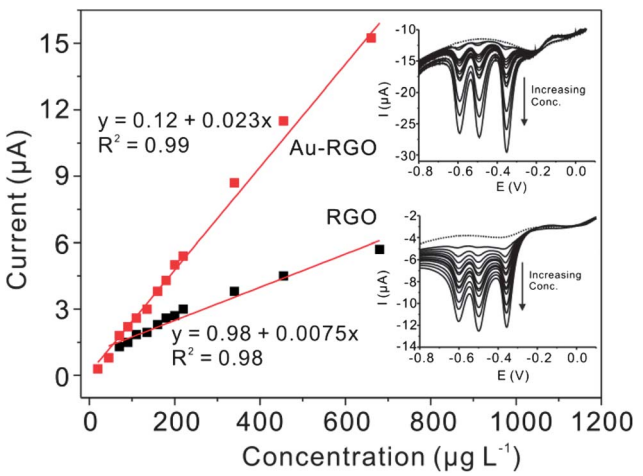

Fig. 7 The calibration plots of Au–RGO and RGO modified electrodes towards TNT at different concentrations in 0.5 M PBS (pH 7.0). The insets are the LSV responses of TNT on Au–RGO (top) and RGO (bottom) modified electrodes.

Table 1 Comparison in detection of seven aromatic compounds on Au–graphene modified GCE[a]

Analytes	Concentration ($\mu g\ L^{-1}$)	Reduction peak	
		E_p (V)	I_p (μA)
TNT	200	−0.35	5.4
		−0.49	3.7
		−0.59	3.9
2,4-DNT	400	−0.53	2.3
		−0.67	1.9
4-NT	800	−0.67	2.4
4-NP	800	−0.73	3.0
Toluene	2000	—	—
Phenol	2000	—	—
Benzene	2000	—	—

[a] 2,4-DNT: 2,4-dinitrotoluene, 4-NT: 4-nitrotoluene, 4-NP: 4-nitrophenol.

Conclusions

A facile and environment-friendly method using UV irradiation was successfully developed for the preparation of an Au–reduced graphene oxide nanocomposite. The results demonstrated that simultaneous reduction of graphene oxide and formation of Au nanoparticles were achieved. The obtained Au nanoparticles with an average diameter of 25.7 nm were uniformly dispersed on graphene sheets. The introduction of Au nanoparticles efficiently maximized the electroactive surface area of catalysts and the conductivity of Au–RGO nanocomposite. The RGO sheets not only provided the nucleation sites but also prevented the Au nanoparticles from agglomeration. The electrochemical sensing performance to TNT was investigated. Good sensitivity (0.023 $\mu A\ \mu g^{-1}\ L$) obtained on Au–RGO modified electrode was found to be superior to that of RGO (0.0075 $\mu A\ \mu g^{-1}\ L$). Initial electrochemical results indicated that the Au–RGO nanocomposite produced can be potentially developed as an electrochemical sensor. Moreover, the UV irradiation technique could be of great benefit for the direct eco-preparation of other graphene-based nanocomposites and fabrication of catalyst-type electrochemical sensors toward more target molecules.

Acknowledgements

This work was supported by the National Key Scientific Program-Nanoscience and Nanotechnology (no. 2011CB933700), and the National Natural Science Foundation of China (no. 61102013 and 90923033). X.-J.H. acknowledges the One Hundred Person Project of the Chinese Academy of Sciences, China, for financial support.

Notes and references

1 K. S. Novoselov, A. K. Geim, S. V. Morozov, D. Jiang, Y. Zhang, S. V. Dubonos, I. V. Grigorieva and A. A. Firsov, *Science*, 2004, **306**, 666.
2 A. A. Balandin, S. Ghosh, W. Z. Bao, I. Calizo, D. Teweldebrhan, F. Miao and C. N. Lau, *Nano Lett.*, 2008, **8**, 902.
3 C. Lee, X. D. Wei, J. W. Kysar and J. Hone, *Science*, 2008, **321**, 385.
4 M. J. McAllister, J. L. Li, D. H. Adamson, H. C. Schniepp, A. A. Abdala, J. Liu, M. Herrera-Alonso, D. L. Milius, R. Car, R. K. Prud'homme and I. A. Aksay, *Chem. Mater.*, 2007, **19**, 4396.
5 C. Berger, Z. M. Song, T. B. Li, X. B. Li, A. Y. Ogbazghi, R. Feng, Z. T. Dai, A. N. Marchenkov, E. H. Conrad, P. N. First and W. A. de Heer, *J. Phys. Chem. B*, 2004, **108**, 19912.
6 Y. Wei, C. Gao, F. L. Meng, H. H. Li, L. Wang, J. H. Liu and X. J. Huang, *J. Phys. Chem. C*, 2012, **116**, 1034.
7 C. Xu, X. Wang and J. W. Zhu, *J. Phys. Chem. C*, 2008, **112**, 19841.
8 Y. C. Si and E. T. Samulski, *Chem. Mater.*, 2008, **20**, 6792.
9 Y. Wang, S. Zhang, D. Du, Y. Y. Shao, Z. H. Li, J. Wang, M. H. Engelhard, J. H. Li and Y. H. Lin, *J. Mater. Chem.*, 2011, **21**, 5319.
10 R. Muszynski, B. Seger and P. V. Kamat, *J. Phys. Chem. C*, 2008, **112**, 5263.
11 G. Goncalves, P. A. A. P. Marques, C. M. Granadeiro, H. I. S. Nogueira, M. K. Singh and J. Gracio, *Chem. Mater.*, 2009, **21**, 4796.
12 B. S. Kong, J. X. Geng and H. T. Jung, *Chem. Commun.*, 2009, 2174.
13 H. Y. Koo, H. J. Lee, Y. Y. Noh, E. S. Lee, Y. H. Kim and W. S. Choi, *J. Mater. Chem.*, 2012, **22**, 7130.
14 Y. Choi, H. S. Bae, E. Seo, S. Jang, K. H. Park and B. S. Kim, *J. Mater. Chem.*, 2011, **21**, 15431.
15 J. Li, C. Y. Liu and Y. Liu, *J. Mater. Chem.*, 2012, **22**, 8426.
16 H. Q. Zhou, C. Y. Qiu, Z. Liu, H. C. Yang, L. J. Hu, J. Liu, H. F. Yang, C. Z. Gu and L. F. Sun, *J. Am. Chem. Soc.*, 2010, **132**, 944.
17 G. L. Li, G. Liu, M. Li, D. Wan, K. G. Neoh and E. T. Kang, *J. Phys. Chem. C*, 2010, **114**, 12742.
18 W. J. Hong, H. Bai, Y. X. Xu, Z. Y. Yao, Z. Z. Gu and G. Q. Shi, *J. Phys. Chem. C*, 2010, **114**, 1822.
19 X. Wang, O. Ramstrom and M. D. Yan, *J. Mater. Chem.*, 2009, **19**, 8944.
20 X. Huang, X. Qi, Y. Huang, S. Li, C. Xue, C. L. Gan, F. Boey and H. Zhang, *ACS Nano*, 2010, **4**, 6196.
21 M. Mandal, S. K. Ghosh, S. Kundu, K. Esumi and T. Pal, *Langmuir*, 2002, **18**, 7792.
22 K. H. Kim, J. U. Kim, S. H. Cha and J. C. Lee, *J. Am. Chem. Soc.*, 2009, **131**, 7482.
23 S. Eustis, H. Y. Hsu and M. A. El-Sayed, *J. Phys. Chem. B*, 2005, **109**, 4811.
24 Y. Matsumoto, M. Koinuma, S. Ida, S. Hayami, T. Taniguchi, K. Hatakeyama, H. Tateishi, Y. Watanabe and S. Amano, *J. Phys. Chem. C*, 2011, **115**, 19280.
25 Y. H. Ding, P. Zhang, Q. Zhuo, H. M. Ren, Z. M. Yang and Y. Jiang, *Nanotechnology*, 2011, **22**, 215601.
26 G. H. Moon, Y. Park, W. Kim and W. Choi, *Carbon*, 2011, **49**, 3454.
27 S. Moussa, G. Atkinson, M. SamyEl-Shall, A. Shehata, K. M. AbouZeid and M. B. Mohamed, *J. Mater. Chem.*, 2011, **21**, 9608.
28 L. Guardia, S. Villar-Rodil, J. I. Paredes, R. Rozada, A. Martinez-Alonso and J. M. D. Tascon, *Carbon*, 2012, **50**, 1014.
29 W. S. Hummers and R. E. Offeman, *J. Am. Chem. Soc.*, 1958, **80**, 1339.
30 H. Zhang, S. Chen, X. Quan, H. T. Yu and H. M. Zhao, *J. Mater. Chem.*, 2011, **21**, 12986.
31 V. Singh, D. Joung, L. Zhai, S. Das, S. I. Khondaker and S. Seal, *Prog. Mater. Sci.*, 2011, **56**, 1178.
32 H. G. Boyen, G. Kastle, F. Weigl, B. Koslowski, C. Dietrich, P. Ziemann, J. P. Spatz, S. Riethmuller, C. Hartmann, M. Moller, G. Schmid, M. G. Garnier and P. Oelhafen, *Science*, 2002, **297**, 1533.
33 R. Zan, U. Bangert, Q. Ramasse and K. S. Novoselov, *Small*, 2011, **7**, 2868.
34 H. J. Yin, H. J. Tang, D. Wang, Y. Gao and Z. Y. Tang, *ACS Nano*, 2012, **6**, 8288.
35 C. C. Li, W. P. Cai, B. Q. Cao, F. Q. Sun, Y. Li, C. X. Kan and L. D. Zhang, *Adv. Funct. Mater.*, 2006, **16**, 83.
36 Y. H. Lee, L. Polavarapu, N. Y. Gao, P. Y. Yuan and Q. H. Xu, *Langmuir*, 2012, **28**, 321.
37 M. Madjet, C. Guet and W. R. Johnson, *Phys. Rev. A*, 1995, **51**, 1327.
38 C. B. Liu, K. Wang, S. L. Luo, Y. H. Tang and L. Y. Chen, *Small*, 2011, **7**, 1203.
39 Y. G. Zhou, J. J. Chen, F. B. Wang, Z. H. Sheng and X. H. Xia, *Chem. Commun.*, 2010, **46**, 5951.
40 B. K. Jena, S. J. Percival and B. Zhang, *Anal. Chem.*, 2010, **82**, 6737.
41 K. Jo, T. Lee, H. J. Choi, J. H. Park, D. J. Lee, D. W. Lee and B. S. Kim, *Langmuir*, 2011, **27**, 2014.
42 Y. X. Xu, H. Bai, G. W. Lu, C. Li and G. Q. Shi, *J. Am. Chem. Soc.*, 2008, **130**, 5856.
43 X. C. Fu, X. Chen, J. Wang, J. H. Liu and X. J. Huang, *Electrochim. Acta*, 2010, **56**, 102.